Impact of growth conditions and strain on indium incorporation in non-polar m-plane $(10\bar{1}0)$ InGaN grown by plasma-assisted molecular beam epitaxy

Alexander Senichev (iD), Brandon Dzuba, Trang Nguyen, Yang Cao, Michael A. Capano, Michael J. Manfra, and Oana Malis (iD)

View Online   Export Citation   CrossMark

ARTICLES YOU MAY BE INTERESTED IN

Impact of growth conditions and strain on indium incorporation in non-polar m-plane $(10\bar{1}0)$ InGaN grown by plasma-assisted molecular beam epitaxy

View Online   Export Citation   CrossMark

Alexander Senichev,[1,2] (iD) Brandon Dzuba,[1,2] Trang Nguyen,[2] Yang Cao,[2] Michael A. Capano,[1,3] Michael J. Manfra,[1,2,3,4] and Oana Malis[2,a] (iD)

AFFILIATIONS

[1] Birck Nanotechnology Center, West Lafayette, Indiana 47907, USA
[2] Department of Physics and Astronomy, Purdue University, West Lafayette, Indiana 47907, USA
[3] School of Electrical and Computer Engineering, Purdue University, West Lafayette, Indiana 47907, USA
[4] School of Materials Engineering, Purdue University, West Lafayette, Indiana 47907, USA

[a] Author to whom correspondence should be addressed: omalis@purdue.edu

ABSTRACT

We establish the relationships between growth conditions, strain state, optical and structural properties of nonpolar m-plane $(10\bar{1}0)$ InGaN with indium composition up to 39% grown by plasma-assisted molecular beam epitaxy. We find that indium mole fraction as a function of growth temperature can be explained by an Arrhenius dependence of InN decomposition only for high temperature and low indium composition InGaN films. For the samples following the Arrhenius behavior, we estimate the effective activation energy for InN thermal decomposition in m-plane InGaN to be about 1 eV. This value is approximately a factor of two smaller than that reported for c-plane InGaN films. At low growth temperatures, InGaN layers show less efficient indium incorporation than predicted by Arrhenius behavior. We attribute the lower than expected indium composition at low temperatures to the strain-induced compositional pulling effect. We demonstrate that at 540 °C, the increase in the InGaN layer thickness leads to a preferential strain relaxation along the a-direction and an increase in the indium composition. For the indium mole fraction up to $x \sim 0.16$, 30-nm-thick m-plane InGaN layers can be coherently grown on GaN with smooth morphology and pronounced low-temperature photoluminescence indicating that the material quality is suitable for device applications.

I. INTRODUCTION

The optical and electronic properties of III-nitride heterostructures that revolutionized the solid state lighting industry also make them promising materials for applications in integrated photonic circuits, passive optical devices, and quantum photonic elements.[1–3] In nitride-based emitters, detectors, and waveguides, InGaN layers play a critical role allowing bandgap tuning through the change of indium composition. The essential material properties of the InGaN alloys, and the III-nitride system generally, were extensively studied in the past for polar c-plane orientation due to the availability of high-quality GaN substrates. However, the growth of nitrides on polar orientations introduces fundamental device design limits related to built-in polarization fields. The fabrication of nitride heterostructures on semipolar and nonpolar GaN planes reduces or eliminates the built-in polarization fields leading to simplified design of devices, enhanced accessible spectral range, reduced distortion of electronic wavefunctions, and increased confinement for high energy states. The fabrication of high-quality films on nonpolar GaN orientations is required to take full advantage of III-nitride heterostructures free of polarization fields.

Specific symmetry and surface termination of the nonpolar substrates impact the growth kinetics and conditions of InGaN epitaxy. Polar c-plane GaN surfaces are typically cation stabilized having only Ga species on top of the surface layer. In this case, the adatom surface interaction is dominated by metallic Ga-Ga bonds resulting in low and isotropic diffusion barriers.[4] Nonpolar m-plane surfaces consist of group III and V species having different bonding properties that along with the atomic geometry of the surface results in a strong in-plane anisotropy with significantly smaller diffusion barriers along the a-direction than along the c-direction.[5] Strong anisotropy in the Ga adatom diffusion barrier and substrate miscut were demonstrated to lead to elongated features on the surface of m-plane GaN grown by plasma-assisted molecular beam epitaxy (PAMBE).[6,7]

The selection of crystal growth orientation also affects the indium incorporation in InGaN. The indium incorporation efficiency was previously compared for polar, nonpolar, and various semipolar InGaN layers grown by metal organic chemical vapor deposition (MOCVD)[8–10] as well as by PAMBE.[11,12] The results on PAMBE-grown InGaN epilayers indicate that the lowest indium incorporation is for nonpolar planes following the relation $(10\bar{1}0) < (20\bar{2}1) \ll (0001)$.[11,12] The low indium incorporation efficiency requires a lower growth temperature for a given indium composition that typically leads to the degradation of epitaxial layers due to the reduced surface adatom mobility. Understanding the mechanisms of indium incorporation in nonpolar InGaN films is essential to improve the material quality at high indium compositions. The studies of nonpolar InGaN layers grown by PAMBE were previously limited to high growth temperatures and low indium compositions <13%.[11,12]

In this work, we study the impact of growth conditions and strain state on the structural and optical properties of InGaN films grown by PAMBE on nonpolar $(10\bar{1}0)$ GaN in the temperature range 450–635 °C. We employ high-resolution x-ray diffraction (XRD) and secondary ion mass spectroscopy (SIMS) to study indium incorporation as a function of temperature. For an accurate assessment of the strain state and composition profile of InGaN films, XRD reciprocal space mapping (RSM) was employed. From the temperature dependence of indium incorporation, we estimate the effective activation energy of thermal InN decomposition for m-plane InGaN. For low-temperature and high indium composition layers, we observe that indium incorporation efficiency is additionally limited by the strain-induced compositional pulling effect. We find that the samples with indium composition up to 16% can be grown coherently to GaN while exhibiting smooth morphology and pronounced low-temperature photoluminescence (PL). The material quality of these m-plane InGaN films makes them promising for device applications.

II. EXPERIMENTAL

InGaN layers were grown by PAMBE on m-plane $(10\bar{1}0)$ oriented free-standing GaN substrates. We used commercially available nonpolar semi-insulating GaN substrates from Nanowin with a nominal threading dislocation density <5 × 10^6 cm^{-2}. The substrate size is 10 mm × 5 mm. The substrates were miscut −0.5° ± 0.2° toward the c-axis (N-polar). The miscut suppresses hillock formation around threading dislocations[13] and leads to an optimal surface morphology of PAMBE-grown m-plane GaN.[7] The average root mean square (rms) roughness of the substrates measured by atomic force microscopy (AFM) on an area 4 × 4 μm^2 was below 0.3 nm.

The m-plane InGaN/GaN heterostructures were grown in a PAMBE system equipped with conventional effusion cells for indium and gallium. The active nitrogen flux was supplied by a Veeco Unibulb radio-frequency plasma source operating at 300 W forward power with 0.5 sccm of nitrogen (N$_2$) flow. The resulting active nitrogen flux of 6.42 × 10^{14} atoms/cm^{2}s was assessed using XRD measurements of the thickness of GaN layers in AlGaN/GaN superlattices grown under metal-rich conditions at 720 °C. The impinging metal fluxes were measured as beam equivalent pressure (BEP) and reported in terms of atomic fluxes. The gallium flux was calibrated through the thickness of low-indium-content InGaN layers grown in the nitrogen-rich regime at growth temperatures <600 °C with the assumption that all gallium is preferentially incorporated. The impinging indium flux was calibrated through the growth of a thick c-plane InN film at a substrate temperature where thermal decomposition and indium adatom desorption are negligible (<435 °C).[14]

Due to the relatively small size of m-plane GaN substrates, they were gallium-mounted to two-inch GaN/Sapphire host wafers to fit a standard MBE sample holder. The host wafers were backside coated with WSi that provides good thermal coupling and temperature uniformity. Before InGaN growth, a 150-nm-thick GaN buffer layer was grown at 720 °C using modulated growth under Ga-rich conditions to ensure a smooth surface. Excess gallium was either incorporated into the GaN lattice or thermally desorbed from the surface during periodic growth interruptions under nitrogen flux and at the end of the buffer layer growth. The surface of the m-plane GaN control sample grown under these conditions (not shown here) was droplet-free with undulations and pronounced stepped terraces characteristic of a miscut in the c-direction similar to previously reported results.[11]

In terms of impinging fluxes, the InGaN growth was performed in the nitrogen-rich regime with a total metal to nitrogen ratio III/V below 1 for all samples (Table I). However, due to the InN thermal decomposition expected at the studied growth temperatures, the actual indium incorporation is typically below the nominal value defined by the impinging fluxes. Indium that was not incorporated into the lattice can either accumulate on the surface or thermally desorb. In this work, we experimentally selected the indium flux

TABLE I. Growth conditions of m-plane InGaN layers at constant Φ_N = 6.4 × 10^{14} atoms/cm^{2}s and Φ_{Ga} = 3.2 × 10^{14} atoms/cm^2 s.

Sample No.	Growth temperature, ±4 °C	Indium flux, atoms/cm^2 s	III/V ratio
A	450	2.4 × 10^{14}	0.88
B	500	1.4 × 10^{14}	0.72
C	540	1.4 × 10^{14}	0.72
D	570	1.0 × 10^{14}	0.66
E	600	1.7 × 10^{14}	0.77
F	635	2.7 × 10^{14}	0.92

to provide slightly more indium than could be both incorporated into InGaN and thermally desorbed from the surface at the studied growth temperatures. The excess indium accumulating on the surface leads to a full metal coverage and eventually to droplet formation. Growth under a full indium coverage was confirmed by the presence of indium droplets on the surface after growth. This growth regime with excess indium on the growth front is referred throughout this paper as an effectively metal-rich regime. A further increase in the indium flux at fixed growth conditions does not change the indium composition that saturates at a maximum value. For samples grown at high temperatures ≥600 °C, droplets were not visible for 30-nm-thick films due to efficient indium desorption. However, the exceptional surface morphology of InGaN films suggests the growth under a metal adlayer at this temperature as well.

A series of 30-nm-thick m-plane InGaN layers were grown at different temperatures 450–635 °C to study the indium incorporation efficiency as a function of temperature. At a growth temperature of 450 °C, the thermal dissociation of InN is expected to be negligible as reported for c-plane InGaN[14] and the indium composition should be close to the nominal value determined by impinging fluxes. At higher growth temperatures, InN dissociation is considered to be the primary factor limiting the indium composition of InGaN alloys. Table I summarizes the growth conditions of the InGaN samples grown by PAMBE. The target growth temperatures are listed, while the actual values measured by a pyrometer varied ±4 °C.

The composition and strain state of InGaN alloys were studied by XRD techniques. The XRD symmetric ω/2θ data was analyzed using the software package Epitaxy 4.5a from PANalytical. The indium content was also assessed by SIMS at EAG Laboratories. The surface morphology of InGaN layers was studied by AFM. The excess indium, including droplets, was removed from the surface by HCl etching before the AFM measurements. For optical characterization, photoluminescence (PL) measurements were performed at liquid nitrogen temperature (~77 K). We used a 325-nm helium-cadmium (He-Cd) laser as the PL excitation source.

III. RESULTS AND DISCUSSION

Figure 1 shows the characteristic surface morphology of m-plane InGaN films grown at different substrate temperatures under effectively metal-rich conditions. The surface of the InGaN sample grown at the highest temperature (sample F, ~635 °C) has a low rms roughness of about 0.2 nm with clear atomic steps (see the supplementary material). The surface morphology is comparable to that of previously reported low indium content high-temperature InGaN films grown on m-plane GaN by PAMBE.[11] The increase in the indium composition achieved by growth at lower temperatures leads to gradual deterioration of the surface morphology. In the temperature range 540–600 °C, the InGaN layers still have low rms roughness in the range of 0.1–0.3 nm, which is comparable to the surface rms roughness of low-temperature m-plane GaN films grown under the metal-rich regime [Fig. 1(a), dashed line]. However, InGaN layers exhibit less pronounced stepped terraces [Fig. 1(b)]. At temperatures below 540 °C, the rms roughness rapidly increases with the appearance of grainy surface morphology [Fig. 1(c)]. We assign the increase in the surface roughness to the decrease in adatom mobility on the surface at reduced temperatures. Even though the low-temperature growth leads to decreased adatom mobility, we speculate that the effectively metal-rich growth conditions act to preserve subnanometer rms roughness.

To determine the indium content of InGaN films grown on GaN, we employed the XRD RSM technique. RSMs can provide information on both the in-plane and out-of-plane lattice constants that allow evaluation of the indium composition profile and strain state for each sample. Asymmetrical RSM measurements were performed using the $(20\bar{2}1)$ and $(21\bar{3}0)$ reflections. From the pair of RSMs, the three different lattice constants for the a-, c-, and m-directions can be directly obtained. Figure 2 shows representative RSMs of $(20\bar{2}1)$ and $(21\bar{3}0)$ reflections for two m-plane InGaN films A and C grown at 450 °C and 540 °C, respectively.

For the InGaN layer grown at 540 °C, the diffraction peak of InGaN is horizontally aligned with that of the GaN layer [Figs. 2(a) and 2(b)]. Specifically, InGaN and GaN layers exhibit peaks with the
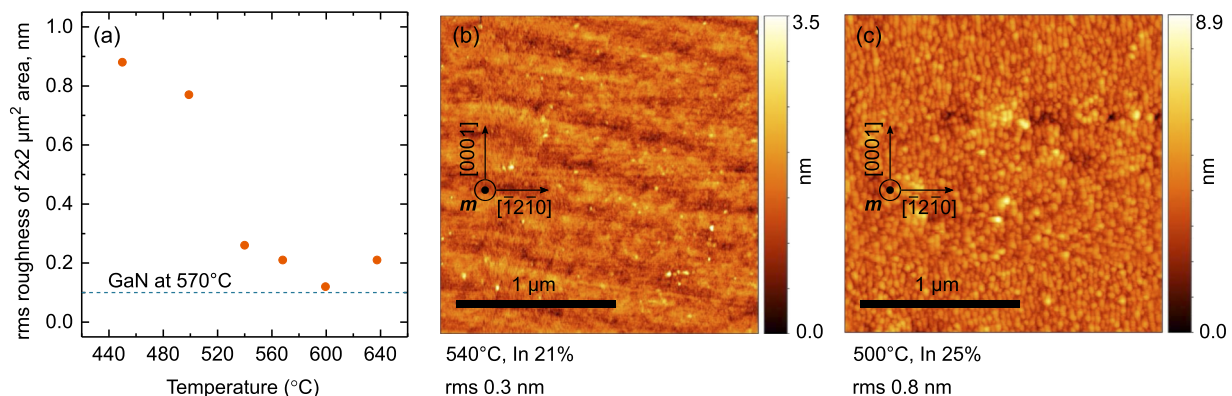
FIG. 1. Surface morphology of m-plane InGaN films grown at different growth temperatures. (a) rms roughness measured from $2 \times 2 \ \mu m^2$ AFM micrographs as a function of growth temperature. The horizontal dashed line indicates the reference rms roughness for a low-temperature GaN film grown at 570 °C under Ga-rich conditions. [(b) and (c)] Representative $2 \times 2 \ \mu m^2$ AFM micrographs of two samples grown at 540 °C (sample C) and 500 °C (sample B), respectively, showing a substantial change of the surface roughness at low growth temperatures.
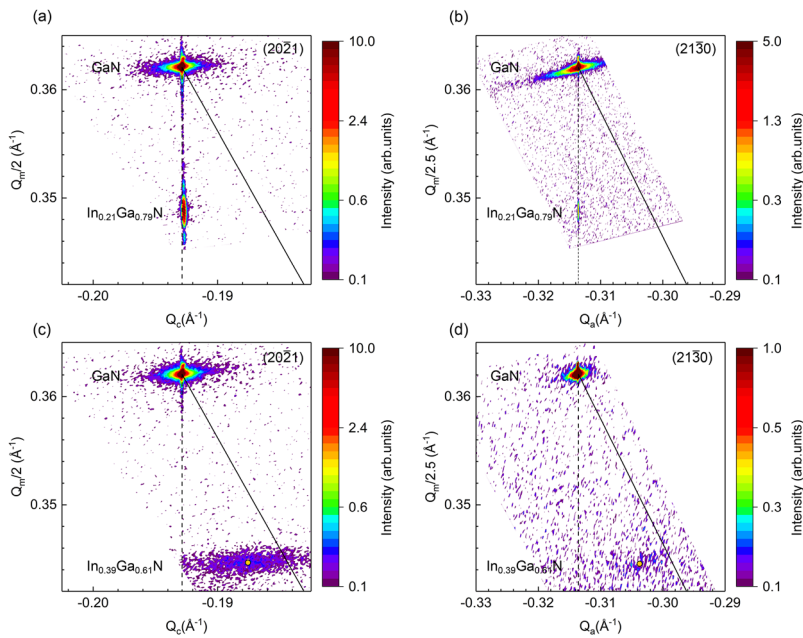
FIG. 2. XRD reciprocal space maps of m-plane $In_xGa_{1-x}N$/GaN samples: (a) and (b) show maps from asymmetric reflections $(20\bar{2}1)$ and $(21\bar{3}0)$, respectively, for the InGaN film grown at 540 °C; (c) and (d) show maps using the $(20\bar{2}1)$ and $(21\bar{3}0)$ reflections, respectively, for the InGaN film grown at 450 °C. The dashed vertical lines indicate the positions of coherently strained $In_xGa_{1-x}N$, and the solid lines indicate the peak positions of fully relaxed $In_xGa_{1-x}N$ along both the a- and c-direction.

same in-plane reciprocal vectors Q_c and Q_a for $(20\bar{2}1)$ and $(21\bar{3}0)$ RSMs, respectively. The images indicate that the InGaN layer is coherently strained to the GaN substrate and has insignificant relaxation in both the c- and a-direction. In turn, the reciprocal lattice point of the InGaN film grown at 450 °C is shifted horizontally with respect to the GaN in-plane reciprocal lattice vector for both $(20\bar{2}1)$ and $(21\bar{3}0)$ RSMs [Figs. 2(c) and 2(d)]. The observed shift is toward the position of the fully relaxed layer (Fig. 2, solid lines). Therefore, the InGaN layer grown at 450 °C is partially relaxed along the c- and a-direction.

The InGaN peak displacement in reciprocal space reveals both indium content and strain state changes. Knowing the strained lattice constants for the a-, c-, and m-directions, the composition and strain state can be estimated making use of recursive calculations described by Shojiki et al.[15] and elastic constants for the GaN and InN binaries.[16] The indium compositions obtained from RSMs for InGaN/GaN heterostructures grown at 450 °C, 540 °C, and 600 °C are 39%, 21%, and 11%, respectively (Fig. 3, open red circles). The calculated strain along the c- and a-direction for the fully strained InGaN layer grown at 540 °C is −1.96% and −2.25%,
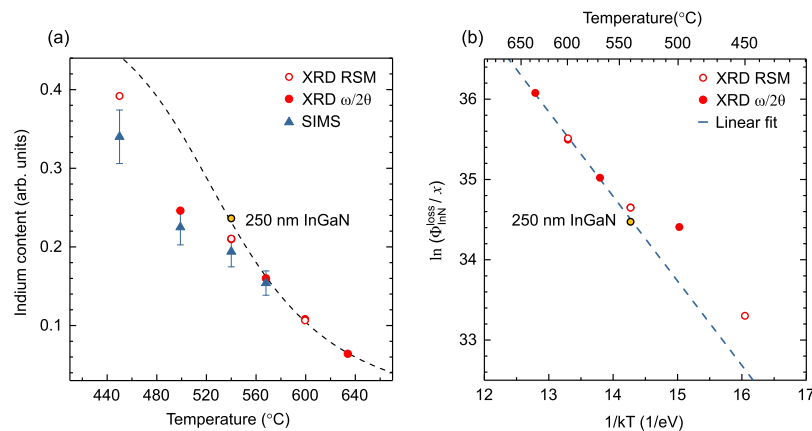
FIG. 3. (a) Indium composition of $(10\bar{1}0)$ InGaN films as a function of growth temperature for $\Phi_N = 6.4 \times 10^{14}$ atoms/cm² s, $\Phi_{Ga} = 3.2 \times 10^{14}$ atoms/cm²s, and indium fluxes given in Table I. The indium composition was assessed by XRD symmetric ω/2θ scans (full red circles), XRD RSMs (open red circles), and SIMS (blue triangles). The error bars indicate the precision of SIMS measurements in providing the relative difference in the indium composition between studied samples, which is ±0.1 of the measured value. (b) Arrhenius plot of the InN losses Φ_{InN}^{loss} normalized to the indium composition x at the given growth temperature. The blue dashed line corresponds to the best fit of experimental data to the equation $\Phi_{InN}^{loss}/x = C \times \exp(-E_a/kT)$ for the high temperature and low indium composition samples. The yellow circles in (a) and (b) show the indium composition and the InN losses of the partially relaxed 250-nm-thick InGaN layer grown at 540 °C, respectively.

respectively. The negative sign indicates that the InGaN layer is under compressive strain since the measured lattice constant is smaller than the relaxed one for the given indium composition. The calculated residual strain for the partially relaxed InGaN layer grown at 450 °C along the c- and a-direction is −1.03% and −0.99%, respectively.

For the sample grown at 540 °C, the estimated indium composition from RSMs is about 21%, while the InGaN layer is coherently strained to the GaN substrate [Figs. 2(a) and 2(b)]. It should be noted that the thickness and composition of this epilayer are above the critical values for the formation of misfit dislocations (MDs) according to the Matthews-Blakeslee model calculated for m-plane InGaN in Ref. 17. However, Hsu et al.[17] also reported that the experimental critical thickness of m-plane InGaN for MDs formation generated by a prismatic slip can be approximately six times larger than the theoretical value. Extrapolation of their results to the 30-nm-thick m-plane $In_{0.21}Ga_{0.79}N$ film indicates that its thickness is slightly above the experimental critical thickness. We speculate that this may result in the low density of MDs and insignificant relief of the misfit strain shown by RSM maps [Figs. 2(a) and 2(b)]. Since the sample grown at 540 °C is coherently strained to the GaN substrate, we assume that all samples grown at a temperature above 540 °C with composition lower than 21% are also coherently strained. Therefore, the indium composition can be estimated via symmetric XRD ω/2θ scans around $(10\bar{1}0)$ Bragg reflection considering coherent growth of InGaN on GaN. The indium composition derived from the symmetric XRD ω/2θ scan for the sample grown at 540 °C is 21%, which agrees with the value obtained from the RSM measurements.

Figure 3(a) summarizes indium composition dependence on temperature assessed by different experimental techniques. The indium compositions derived from RSM are shown in open red circles. The indium compositions estimated from symmetric ω/2θ XRD scans are shown in full red circles. Furthermore, the indium composition was analyzed by the strain independent SIMS technique (Fig. 3, blue triangles). Even though SIMS absolute values are only accurate to ±0.2 of the measured value, the technique is capable of providing the relative difference in indium composition between studied samples with the confidence of ±0.1 (Fig. 3, error bars). We found that the trend given by SIMS is in very good agreement with composition estimates made by XRD. As expected, the decrease in the growth temperature leads to a continuous increase in the indium content due to the reduced rate of InN decomposition at a given nitrogen flux. Moreover, all samples show an indium composition lower than that of the semipolar and polar InGaN films in agreement with previous findings.[11,18]

Knowing the temperature dependence of indium incorporation, the activation energy of InN thermal decomposition can be found. From the actual indium composition estimated by XRD techniques, we derived the InN losses Φ_{InN}^{loss} as a function of temperature making use of procedures described in Refs. 18–20. The obtained values of Φ_{InN}^{loss} normalized to the indium composition x are plotted in Fig. 3(b) using a semilogarithmic scale. The temperature dependence of Φ_{InN}^{loss} can be well described by an Arrhenius equation of the following form:

$$\Phi_{InN}^{loss} = C \times x \times \exp(-E_a/kT), \quad (1)$$

where C is a constant, E_a is the activation energy, and k is the Boltzmann factor.[18,20] From Eq. (1), the $\ln(\Phi_{InN}^{loss}/x)$ is a linear function of $1/T$, where T is the growth temperature. We fitted our experimental data in Fig. 3(b) with Eq. (1) and found that only high temperature and low indium composition InGaN layers show a linear dependence. For samples grown at temperatures below 540 °C, it can be noted that $\ln(\Phi_{InN}^{loss}/x)$ values deviate from the linear dependence indicating higher InN losses, i.e., lower indium incorporation than predicted by the Arrhenius function.

The deviation from the Arrhenius temperature dependence suggests a change in mechanism limiting indium incorporation in m-plane InGaN films grown at low temperatures. An incremental increase in indium composition caused by a reduced InN thermal dissociation increases in-plane compressive strain between the InGaN layer and the GaN host substrate. This mismatch strain partially suppresses additional incorporation of indium atoms in InGaN alloys in what is known as the compositional pulling effect.[21,22] The phenomenon consists of a reduction of the lattice mismatch strain energy through pulling the alloy composition toward lattice matching. Therefore, at low temperatures, the indium incorporation is determined by the compositional pulling effect in addition to the InN thermal decomposition leading to deviation from the Arrhenius dependence [Fig. 3(b)].

To confirm that the observed partial suppression of indium incorporation is due to this phenomenon, we compared the indium composition of two samples grown under the same growth conditions but having different thicknesses. The 30-nm-thick InGaN layer (sample C, 540 °C) is coherently strained to GaN and has the indium composition of about 21% [Figs. 2(a) and 2(b)]. A 250-nm-thick InGaN layer grown at the same temperature shows partial relaxation only along the a-axis and the indium composition ~24%. The detailed RSM analysis of the thick InGaN layer is provided in the supplementary material. The increase in indium incorporation upon strain relaxation supports the assignment of the deviation from the Arrhenius temperature function to the compositional pulling effect. We calculated the InN losses Φ_{InN}^{loss} for the 250-nm-thick InGaN layer and plotted in Fig. 3(b) (yellow circle). As can be seen, the resulted value for $\ln(\Phi_{InN}^{loss}/x)$ for the partially relaxed layer is shifted now toward the values predicted by the Arrhenius dependence.

Moreover, it can be noted that the deviation from the Arrhenius dependence in Fig. 3(b) of sample A (450 °C) is comparable to that of sample B (500 °C), even though the former has a higher indium composition and hence should experience a stronger impact of the compositional pulling effect. However, the RSM measurements indicate a partial strain relaxation of the InGaN layer in sample A of about 72% and 76% along the c- and a-axes, respectively [Figs. 2(c) and 2(d)]. The strain relaxation leads to a reduction of the compositional pulling effect and an increase in the indium composition toward the values given by the impinging fluxes and the Arrhenius dependence.

From fitting of the experimental data for high temperature and low indium composition InGaN samples with an Arrhenius behavior, we derived the activation energy of InN thermal dissociation. It should be noted that the analysis of the experimental results is limited to a few data points due to the composition pulling effect. Moreover, the indium incorporation at high temperatures can be partially affected by the composition pulling effect as well.

Therefore, we refer to the obtained value as the effective activation energy E_a^{eff} of InN thermal dissociation for nonpolar ($10\bar{1}0$) InGaN. From the slope of the Arrhenius function, we found the E_a^{eff} equal to ~1 eV. In the work of Gačević *et al.*,[18] it was found that thermal decomposition of polar c-plane InGaN can be well described by an Arrhenius function with the activation energy of 1.84 ± 0.12 eV comparable to that obtained for binary InN layers.[14] Our results show a value that is lower by about a factor of two than the one previously reported for c-plane InGaN alloys,[18–20,23] and the theoretical prediction for In-N bond energy of 1.93 eV.[24] This low activation energy for InN dissociation during m-plane growth might explain the substantially lower indium incorporation in comparison with polar (0001) InGaN that has been previously reported.[11]

Figure 3(a) (dashed line) plots the expected temperature dependence of indium composition using the activation energy of InN thermal decomposition extracted from Fig. 3(b). We found that the calculated indium composition at 450 °C is below the nominal value x~0.5 given by the impinging gallium and nitrogen fluxes. However, at this growth temperature, the InN thermal decomposition has been reported to be negligible for the c-plane orientation.[14] This indicates that the onset of InN thermal decomposition happens at lower temperatures for nonpolar m-plane than for c-plane InGaN grown by PAMBE.

To assess the optical quality of m-plane epilayers, InGaN films of different compositions were characterized by low-temperature PL measurements. Figure 4 shows the normalized PL spectra of the InGaN layers recorded at ~79 K. The PL peak energy monotonically shifts to lower values with the increase in the indium composition, whereas the full width at half maximum (FWHM) shows a weak dependence on the alloy composition. The FWHM of the PL peaks is 73 meV, 60 meV, and 79 meV for InGaN layers with the InN mole fraction of 0.06 (F), 0.11 (E), and 0.16 (D), respectively (Fig. 4). For InGaN layers with indium composition ≥21%, a very weak PL signal was detected even at the liquid-nitrogen temperature. We attribute the decrease in the PL intensity to the higher density of defects
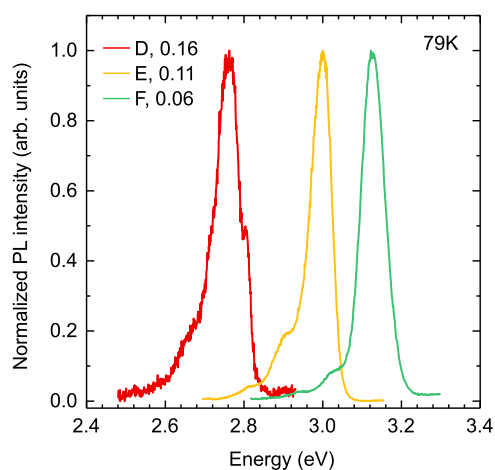
in low temperature growth of high indium composition samples. Increased indium incorporation at low temperatures leads to larger strain accumulation, which can be partially released through defect formation once the critical thickness of the epilayers is reached.[17] Overall, the m-plane InGaN films with indium composition up to 16% grown by PAMBE on ($10\bar{1}0$) GaN under the effectively metal-rich regime are coherently strained and show a smooth surface with low rms roughness and pronounced PL emission at low temperatures. The obtained material properties are suitable for fabrication of m-plane InGaN-based heterostructures for application in devices free of polarization fields.

IV. CONCLUSION

In conclusion, we studied the interplay between growth conditions, strain state, and resulting structural and optical properties of InGaN films grown by PAMBE on nonpolar ($10\bar{1}0$) GaN in the temperature range 450–635 °C. We demonstrated that the growth under the effectively metal-rich regime provides the surface morphology of InGaN layers with exceptionally low rms roughness for growth temperatures as low as 540 °C. Moreover, XRD RSM measurements showed that these InGaN layers are coherently strained to GaN. At lower growth temperatures, surface roughening was observed due to the strain relaxation and reduced surface adatom mobility even in the presence of excess indium surface coverage. From the accurate assessment of alloy composition by different techniques, we found that the InN decomposition can be well described by an Arrhenius dependence only for high temperature and low indium composition InGaN films. At low growth temperatures, InGaN layers show less efficient indium incorporation deviating from the expected temperature function. We attribute the decrease in the incorporation rate to the compositional pulling effect that becomes more prominent in the InGaN films with a higher indium composition. Therefore, the determination of the activation energy E_a is intrinsically limited to a narrow temperature range due to the compositional pulling effect. From the samples following the Arrhenius temperature function, we found an effective activation energy E_a^{eff} of the InN thermal decomposition in nonpolar InGaN of about 1 eV that is about a factor of two smaller than E_a reported for polar c-plane layers. The obtained results explain the previously reported relation for the indium incorporation on different crystal orientations ($10\bar{1}0$) << (0001).

FIG. 4. Normalized PL spectra of the InGaN samples D, E, and F taken at 79 K. The indium contents of the InGaN layers are indicated.

REFERENCES

[1] C. Shen, T. K. Ng, J. T. Leonard, A. Pourhashemi, H. M. Oubei, M. S. Alias, S. Nakamura, S. P. Denbaars, J. S. Speck, A. Y. Alyamani, M. M. Eldesouki, and B. S. Ooi, ACS Photonics **3**, 262 (2016).

[2] X. Gao, Z. Shi, Y. Jiang, S. Zhang, C. Qin, J. Yuan, Y. Liu, P. Grünberg, and Y. Wang, Opt. Lett. **42**, 4853 (2017).

[3] S. T. Jagsch, N. V. Triviño, F. Lohof, G. Callsen, S. Kalinowski, I. M. Rousseau, R. Barzel, J. F. Carlin, F. Jahnke, R. Butté, C. Gies, A. Hoffmann, N. Grandjean, and S. Reitzenstein, Nat. Commun. **9**, 564 (2018).

[4] T. Zywietz, J. Neugebauer, and M. Scheffler, Appl. Phys. Lett. **73**, 487 (1998).

[5] L. Lymperakis and J. Neugebauer, Phys. Rev. B **79**, 241308 (2009).

[6] M. Sawicka, H. Turski, M. Siekacz, J. Smalc-Koziorowska, M. Kryśko, I. Dzięcielewski, I. Grzegory, and C. Skierbiszewski, Phys. Rev. B **83**, 245434 (2011).

[7] J. Shao, L. Tang, C. Edmunds, G. Gardner, O. Malis, and M. Manfra, J. Appl. Phys. **114**, 023508 (2013).

[8] Y. Zhao, Q. Yan, C.-Y. Huang, S.-C. Huang, P. Shan Hsu, S. Tanaka, C.-C. Pan, Y. Kawaguchi, K. Fujito, C. G. Van de Walle, J. S. Speck, S. P. DenBaars, S. Nakamura, and D. Feezell, Appl. Phys. Lett. **100**, 201108 (2012).

[9] T. Wernicke, L. Schade, C. Netzel, J. Rass, V. Hoffmann, S. Ploch, A. Knauer, M. Weyers, U. Schwarz, and M. Kneissl, Semicond. Sci. Technol. **27**, 024014 (2012).

[10] M. Monavarian, A. Rashidi, and D. Feezell, Phys. Status Solidi **216**, 1800628 (2018).

[11] M. Sawicka, A. Feduniewicz-Żmuda, M. Kryśko, H. Turski, G. Muziol, M. Siekacz, P. Wolny, and C. Skierbiszewski, J. Cryst. Growth **459**, 129 (2017).

[12] M. Sawicka, P. Wolny, M. Kryśko, H. Turski, K. Szkudlarek, S. Grzanka, and C. Skierbiszewski, J. Cryst. Growth **465**, 43 (2017).

[13] A. Hirai, Z. Jia, M. C. Schmidt, R. M. Farrell, S. P. Denbaars, S. Nakamura, J. S. Speck, and K. Fujito, Appl. Phys. Lett. **91**, 191906 (2007).

[14] C. S. Gallinat, G. Koblmüller, J. S. Brown, and J. S. Speck, J. Appl. Phys. **102**, 064907 (2007).

[15] K. Shojiki, T. Hanada, T. Shimada, Y. Liu, R. Katayama, and T. Matsuoka, Jpn. J. Appl. Phys., Part 2 **51**, 04DH01 (2012).

[16] A. F. Wright, J. Appl. Phys. **82**, 2833 (1997).

[17] P. S. Hsu, M. T. Hardy, E. C. Young, A. E. Romanov, S. P. Denbaars, S. Nakamura, and J. S. Speck, Appl. Phys. Lett. **100**, 171917 (2012).

[18] Ž. Gačević, V. J. Gómez, N. G. Lepetit, P. E. D. Soto Rodríguez, A. Bengoechea, S. Fernández-Garrido, R. Nötzel, and E. Calleja, J. Cryst. Growth **364**, 123 (2013).

[19] M. Siekacz, M. Sawicka, H. Turski, G. Cywiński, A. Khachapuridze, P. Perlin, T. Suski, M. Bóckowski, J. Smalc-Koziorowska, M. Kryśko, R. Kudrawiec, M. Syperek, J. Misiewicz, Z. Wasilewski, S. Porowski, and C. Skierbiszewski, J. Appl. Phys. **110**, 063110 (2011).

[20] R. Averbeck and H. Riechert, Phys. Status Solidi **176**, 301 (1999).

[21] G. B. Stringfellow, J. Cryst. Growth **312**, 735 (2010).

[22] Y. Inatomi, Y. Kangawa, T. Ito, T. Suski, Y. Kumagai, K. Kakimoto, and A. Koukitu, Jpn. J. Appl. Phys., Part 1 **56**, 078003 (2017).

[23] H. Turski, M. Siekacz, Z. R. Wasilewski, M. Sawicka, S. Porowski, and C. Skierbiszewski, J. Cryst. Growth **367**, 115 (2013).

[24] *Properties of Group III Nitrides*, edited by J. H. Edgar (INSPEC, Institution of Electrical Engineers, 1994).